Ultrasound in Med. & Biol., Vol. 40, No. 4, pp. 675–684, 2014
Copyright © 2014 World Federation for Ultrasound in Medicine & Biology
Printed in the USA. All rights reserved
0301-5629/$ - see front matter

http://dx.doi.org/10.1016/j.ultrasmedbio.2013.10.023

● *Original Contribution for the Festschrift in honor of Robert C. Waag*

THE GAUSSIAN SHEAR WAVE IN A DISPERSIVE MEDIUM

KEVIN J. PARKER* and NATALIE BADDOUR†

* Department of Electrical and Computer Engineering, University of Rochester, Rochester, New York, USA; and † Department of Mechanical Engineering, University of Ottawa, Ottawa, Ontario, Canada

(*Received* 31 *January* 2013; *revised* 29 *October* 2013; *in final form* 30 *October* 2013)

Abstract—In "imaging the biomechanical properties of tissues," a number of approaches analyze shear wave propagation initiated by a short radiation force push. Unfortunately, it has been experimentally observed that the displacement-versus-time curves for lossy tissues are rapidly damped and distorted in ways that can confound simple tracking approaches. This article addresses the propagation, decay and distortion of pulses in lossy and dispersive media, to derive closed-form analytic expressions for the propagating pulses. The theory identifies key terms that drive the distortion and broadening of the pulse. Furthermore, the approach taken is not dependent on any particular viscoelastic model of tissue, but instead takes a general first-order approach to dispersion. Examples with a Gaussian beam pattern and realistic dispersion parameters are given along with general guidelines for identifying the features of the distorting wave that are the most compact. (E-mail: kevin.parker@rochester.edu) © **2014 World Federation for Ultrasound in Medicine & Biology.**

Key Words: **Shear wave, Attenuation, Dispersion, Radiation force, Distortion, Propagation.**

INTRODUCTION

There has been extensive development of techniques to estimate and image the elastic properties of tissues (Doyley 2012; Parker et al. 2011). These provide useful biomechanical and clinically relevant information not available from conventional radiology. A subset of techniques use short-duration pushing pulses of acoustic radiation force as an initial condition, which then results in a propagating shear wave. By tracking the propagating wave, the shear velocity can be estimated, and this yields the Young's modulus or stiffness of the material (Sarvazyan et al. 1998). An impressive set of approaches employing radiation force, with important clinical applications, have been developed (Fatemi and Greenleaf 1998; Hah et al. 2012; Hazard et al. 2012; Konofagou and Hynynen 2003; McAleavey and Menon 2007; Nightingale et al. 1999, 2001; Parker et al. 2011).

Unfortunately, in many lossy tissues, a propagating shear wave produced by a focused ultrasound beam radiation force will rapidly devolve. Specifically, within a few millimeters, the observed displacements are significantly attenuated. Furthermore, the displacement wave has an extended "tail," and the shape becomes distorted. These effects complicate attempts to track the key features of the propagating pulse to estimate shear velocity. As an example, see Figure 1, where an approximately Gaussian axis-symmetric beam at 5 MHz is used to produce a short radiation force push in a gelatin phantom. The displacement versus radial position at the focal depth is illustrated for regular intervals of time after the radiation force push. Even in this case, where gelatin is a relatively elastic (very weakly attenuating and dispersive) medium, the loss of amplitude from cylindrical spreading is pronounced. The long tail of the displacement and softening of the leading edge are evident, even in this "best case" scenario of a low-loss medium. In more lossy tissues, these factors are more pronounced. Analytical and numerical models have been proposed to model the evolution and decay of pulses in viscoelastic media (Bercoff et al. 2004a; Fahey et al. 2005; Nightingale et al. 1999; Sarvazyan et al. 1998). However, there is still the need for a closed-form analytical solution that clearly identifies the key terms responsible for the distortion and decay of the pulse. Furthermore, there are different models for wave propagation in lossy media (Bercoff et al. 2004b; Chen et al. 2004; Chen and Holm 2003, 2004; Giannoula and Cobbold 2008, 2009; Szabo 1994; Urban et al. 2009). As the precise model and mechanism of loss for shear waves in tissue remain

Address correspondence to: Kevin J. Parker, University of Rochester, Hopeman Building 203, P.O. Box 270126, Rochester, NY 14627-0126, USA. E-mail: kevin.parker@rochester.edu

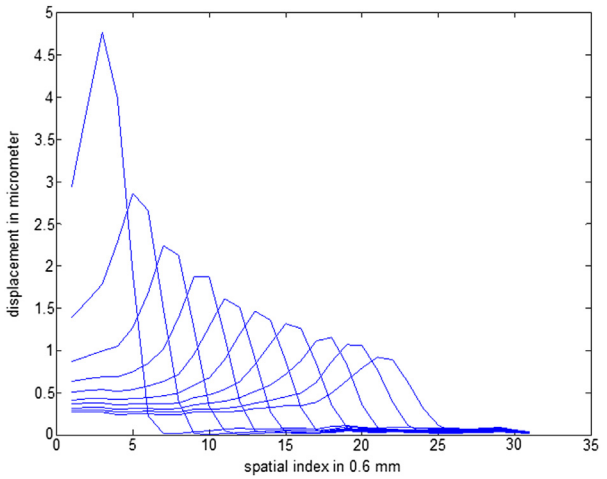

Fig. 1. Experimental data demonstrating the displacements (vertical axis) in a gelatin phantom at different radial positions (horizontal axis) at 1-ms, 2-ms, 3-ms,… intervals after a short radiation force pulse at 5 MHz. The displacements were calculated from tracking scans taken after the radiation force push. An approximately Gaussian, axially symmetric beam pattern was produced at the focal depth with a standard deviation of approximately 1 mm. In a low-loss, low-dispersion medium such as gelatin, the amplitude loss is due largely to cylindrical spreading. Still, the long tail of the displacement curves and softening of the leading edge can be seen. Decay and distortion of the propagating wave are more pronounced in lossy tissues.

uncertain, it is useful to have analytical expressions that are independent of any particular model, but still valid over the operating range of shear wave frequencies.

The Gaussian shape is of particular importance because of a number of fortunate properties. First, the Gaussian function is an eigenfunction of many linear operators including the Fourier transform. Related to this, a focused ultrasound transducer with Gaussian apodization will produce a focal region that has a Gaussian shape in the transverse direction. If this intensity distribution is used to create a radiation force excitation in an absorbing medium, the initial body forces will have a corresponding Gaussian distribution in the axial direction. If a shear wave with Gaussian characteristics can be launched by these means, this wave could be characterized by three parameters: amplitude, position of the centroid and spread. However, dispersion or frequency dependence of wave speed and attenuation will act on the Gaussian pulse to distort its shape, complicating any simple relations and estimators derived in the case of a purely elastic (lossless) medium. In this article, we first treat the idealized 1-D case of a Gaussian shear wave generated by radiation force, then move to the more realistic but more intractable case of an axis-symmetric beam in cylindrical coordinates. We make use of the unifying mathematical framework and fundamental theorems derived recently by Baddour (2011). In some cases, approximate solutions are derived where exact analytical solutions are not found. In all cases, the goal is to elucidate the key factors that reshape a propagating Gaussian pulse, and reduce these to closed-form solutions that are valid in a dispersive media, even when the precise viscoelastic model is uncertain.

THEORY

The 1-D solution

We begin with a 1-D solution based on the experimental configuration illustrated in Figure 2. An ultrasound beam has a Gaussian intensity profile given by

$$I(x) = (1/\sigma)\mathbf{e}^{-\left(x^2/2\sigma^2\right)} \tag{1}$$

in the x-direction, and extends nearly uniformly in the axial (z) direction. This approximates a high f-number beam, propagating in a weakly attenuating medium. The beam is extended in the y-dimension. The initial conditions are that velocity and displacement are everywhere zero, in an infinite, homogeneous medium. We will assume that given the direction and extent of the radiation force, the resulting displacements are polarized in the z-dimension, and the derivatives with respect to y and z are zero. Thus, these conditions lead to an approximation of a 1-D plane wave solution after a temporal impulse of radiation force. Using notation from Graff (1975), we write the governing equation in an elastic medium as

$$\nabla^2 u_z(x,t) - \frac{1}{c^2}\frac{\partial^2 u_z(x,t)}{\partial t^2} = -F_z(x)T(t) \tag{2}$$

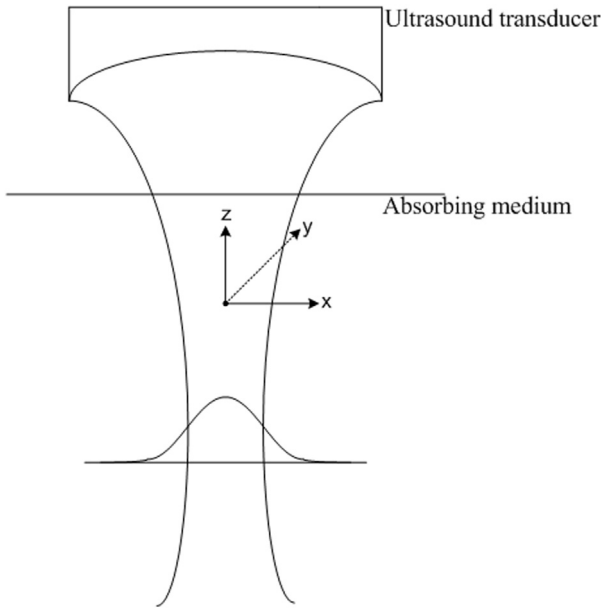

Fig. 2. Schematic of a Gaussian beam, high f-number, applied in an absorbing medium to produce a radiation force push.

where u_z = displacement of shear wave in z-direction; F_z = applied body force, which is proportional to radiation force, $2\alpha_L I(x)/c_L$; $T(t)$ = temporal application, which we will take as an impulse, $\delta(t)$; and α_L and c_L = longitudinal wave (ultrasound) attenuation and wave speed in the medium, respectively. The gradient reduces in this problem to a second derivative in x.

The version of the Fourier transform that we use is defined as follows. Under the suitability of integration of the function $f(t)$, the temporal Fourier transform is defined as $F(\omega) = \int_{-\infty}^{\infty} f(t)\mathbf{e}^{-i\omega t}dt$. The temporal inverse Fourier transform is given by $f(t) = (1/2\pi)\int_{-\infty}^{\infty} F(\omega)\mathbf{e}^{+i\omega t}d\omega$. The Fourier transform can also be applied to the spatial variables. In one dimension, the forward and inverse spatial Fourier transforms are defined as for the temporal transform, with the spatial variable x replacing the temporal variable t in the definition, and the spatial frequency ρ replacing the temporal frequency ω. It is noted that various other conventions are possible regarding the location of the positive and negative signs of the complex exponential kernel, as well as for the placement of the factors of 2π in the forward or inverse Fourier transform. This particular convention for the Fourier transform is the nonunitary version that uses angular frequency (as opposed to ordinary frequency).

Taking the *spatial* Fourier transform of eqn (2) followed by a *temporal* Fourier transform leads to

$$-\rho^2 \widehat{U}_z(\rho,\omega)+k^2 \widehat{U}_z(\rho,\omega) = -\widehat{F}_z(\rho) \tag{3}$$

where, on the right side of the equation, the temporal Fourier transform of the impulse function yields unity, the overhat indicates a temporal Fourier transform, k = wavenumber (= ω/c in a lossless medium); ρ = spatial frequency corresponding to the spatial variable x; and $-\widehat{F}_z(\rho)$ = spatial Fourier transform of $F_z(x)$. Rearranging yields the sinusoidal Green's function

$$\widehat{u}_z(x,\omega) = \Im_\rho^{-1}\left\{\frac{\widehat{F}_z(\rho)}{\rho^2-k^2}\right\} \tag{4}$$

where $\Im_\rho^{-1}\{\bullet\}$ = inverse Fourier transform of the *spatial* frequency variable, ρ. This inverse transform can be difficult to obtain. However, recently, Baddour (2011) reported a set of theorems applicable to 1-, 2- and 3-D wave sources that provide a solution for this type of transform. Specifically, Baddour's (2011) Theorem 5 indicates that the following results are true:

$$\begin{aligned}\Im_\rho^{-1}\left\{\frac{\widehat{F}_z(\rho)}{\rho^2-k^2}\right\} &= \frac{1}{2\pi}\int_{-\infty}^{\infty}\frac{\widehat{F}_z(\rho)}{\rho^2-k^2}\mathbf{e}^{i\rho x}d\rho \\ &= \frac{-i}{2k}\widehat{F}_z(-k)\mathbf{e}^{-ikx} \quad \text{for} \quad x>0\end{aligned} \tag{5}$$

This new theorem effectively takes the spatial source transform $\widehat{F}_z(\rho)$ and converts it to a temporal spectrum, $\widehat{F}_z(-\omega/c)$, a spatial-temporal transformation involving the speed of the shear wave, c. Theorem 5 is applicable to analytical functions, $\widehat{F}_z(\rho)$, that remain bounded, meaning they have no poles. If $\widehat{F}_z(\rho)$ has poles, then a simple application of a partial fraction expansion is required before application of Theorem 5 to separate the poles of $\widehat{F}_z(\rho)$ from the $(\rho^2 - k^2)^{-1}$ term.

Now, let us examine the velocity, $v_z(x,\omega)$:

$$\widehat{v}_z(x,\omega) = i\omega\widehat{u}(x,\omega) = +\frac{c}{2}\widehat{F}_z(-k)\mathbf{e}^{-ikx} \tag{6}$$

So if $F_z(x)$ is a Gaussian, then its spatial Fourier transform, $\widehat{F}_z(\rho)$, is also a Gaussian, and so is $\widehat{F}_z(-k)$ by Baddour's theorem. Thus, $\widehat{v}_z(x,\omega)$ is a Gaussian with phase shift proportional to $-kx = -(x/c)\omega$, which, in turn, corresponds to a shift in time from t to $t - x/c$. Note that, in accordance with D'Alembert's solution for an initial force, it is v and not u that propagates the form of $F_z(x)$ (Graff 1975; Blackstock 2000).

The Fourier transform of $F_z(x) = (1/\sigma)\mathbf{e}^{-x^2/2\sigma^2}$ is given by

$$F_z(\rho) = \sqrt{2\pi}\mathbf{e}^{-\sigma^2\rho^2/2}$$

Therefore, taking the inverse temporal transform of eqn (6), assuming $\widehat{F}_z$ is a Gaussian of magnitude P, yields

$$v_z(x,t) = +\frac{Pc^2}{2\sigma}\,\mathbf{e}^{-(x-ct)^2/2\sigma^2} \tag{7}$$

which agrees with the D'Alembert's solution for the right-traveling wave. The displacement wave $u_z(x, t)$, being the time integration of velocity, is an $\mathrm{Erf}[(x-ct)/\sqrt{2}\sigma\,]$ function that never returns to zero in theory, consistent with the discussions in Blackstock (2000) and Graff (1975). However, in practice, displacements will return to zero by a combination of reflections from boundaries and/or restorative forces. These are low-frequency or long-time phenomena that are difficult to know *a priori*. Background vibration and baseline drift add to the uncertainties. For these reasons, the tracking of displacement is seen to be inferior to the tracking of velocity.

In fact, we can consider that in a very general sense the inverse Fourier transform of eqn (6), where the inverse transform takes the temporal frequency variable ω and transforms to time, t. We recall that $k = \omega/c$ and make use of the Fourier shift and scaling theorems in taking the inverse Fourier transform of eqn (6) to obtain

$$v_z(x,t) = +\frac{c^2}{2}F_z\left(-c\left(t-\frac{x}{c}\right)\right) = \frac{c^2}{2}F_z(x-ct) \quad \text{for} \quad x>0 \tag{8}$$

The preceding equation states very simply and concisely that the original shape of the forcing function is propagated outward (toward increasing x, to the right in this case) and is *unchanged* by the velocity wave. As previously stated, the displacement wave $u(x,t)$, is a time integration of velocity, and thus, the displacement wave would not have the same shape as the original forcing function. Furthermore, the temporal Fourier transform of $v_z(x,t)$, or its bandwidth, is related by eqns (5)–(8) to the beam pattern shape that produces $F_z(x)$. That is, narrow beam patterns produce sharper $v_z(x,t)$, composed of higher bandwidths. Experimental work with focused ultrasound typically produces bandwidths under 1000 Hz, peaking below 500 Hz (McAleavey and Menon 2007; Hah et al. 2012).

Now consider the more relevant case of a medium with attenuation and dispersion. As discussed in Blackstock (2000:ch 9), a variety of loss mechanisms exist in materials, each with their own particular frequency-dependent solution. However, even if the precise mechanism is unknown, the harmonic plane wave solution can be generalized by a complex wavenumber such that the general solution is

$$u_z(x,t) = u_0 \mathbf{e}^{-ikx}\mathbf{e}^{i\omega t} \tag{9}$$

where the wavenumber k is defined such that its imaginary part is negative. Whatever the underlying mechanisms, these parameters will be frequency dependent, and the particular form of frequency dependence will depend strictly on the underlying mechanism expressed in the constitutive equations. Of course, it must be kept in mind that the dispersion of velocity, and attenuation, is linked by Kramers-Kronig relations (Nachman et al. 1990; Szabo 1994; Blackstock 2000).

In this treatment, we are agnostic as to the precise mechanism and, therefore, the extended frequency dependence of the attenuation and phase velocity. Furthermore, we assume that only a limited shear wave frequency bandwidth is available so that any particular frequency dependence can be expressed using a Taylor series expansion over the restricted frequency range.

We therefore begin with a complex wavenumber, setting $k = \omega/c - i\alpha$, where α is the absorption coefficient. The statement corresponding to eqn (5) for complex wave numbers comes from the application of Theorem 6 (complex wavenumber with negative imaginary part) from Baddour (2011), which states:

$$\frac{1}{2\pi}\int_{-\infty}^{\infty}\frac{\widehat{F}_z(\rho)}{\rho^2-k^2}\mathbf{e}^{i\rho x}d\rho = \frac{-i}{2k}\widehat{F}_z(-k)\mathbf{e}^{-ikx} \quad \text{for} \quad x>0 \tag{10}$$

With our choice of negative real part for the complex k, Baddour's Theorem 6 ensures that eqns (4) and (5) are still valid for complex k. Hence, for F_z, a Gaussian of amplitude $P = 1$, eqns (4) and (5) and $\widehat{v}_z(x,\omega) = i\omega\widehat{u}(x,\omega)$ yield

$$\begin{aligned} v_z(x,\omega) &= \frac{\omega}{2k}\,\mathbf{e}^{-\frac{1}{2}\sigma^2k^2}\mathbf{e}^{-ikx} \\ &= \frac{\omega c}{2(\omega - i\alpha c)}\,\mathbf{e}^{-\frac{1}{2}\sigma^2\left(\left(\frac{\omega}{c}\right)^2+\alpha^2\right)}\mathbf{e}^{-i\left(\frac{\omega}{c}\right)x}\mathbf{e}^{-\alpha x} \end{aligned} \tag{11}$$

where we have taken k^2 as the product of its conjugate roots.

Now, assuming weak attenuation, $\alpha << \omega/c$, over most of the bandwidth, we neglect the imaginary term in the denominator and, to first order, we have

$$v_z(x,\omega) \cong \frac{c}{2}\,\mathbf{e}^{-\frac{1}{2}\sigma^2\left[\left(\frac{\omega}{c}\right)^2+\alpha^2\right]}\mathbf{e}^{-i\left(\frac{\omega}{c}\right)x}\mathbf{e}^{-\alpha x} \tag{12}$$

Using the fact that the Fourier transform of

$$F_z(t) = \frac{1}{\sigma\sqrt{2\pi}}\,\mathbf{e}^{-\frac{t^2}{2\sigma^2}}$$

is given by

$$\widehat{F}_z(\omega) = \mathbf{e}^{-\frac{\sigma^2\omega^2}{2}}$$

and taking the temporal inverse Fourier transform yields

$$v(x,t) = \frac{c^2}{2\sigma\sqrt{2\pi}}\,\mathbf{e}^{\frac{-(x-ct)^2}{2\sigma^2}}\mathbf{e}^{\frac{-\sigma^2\alpha^2}{2}}\mathbf{e}^{-\alpha x} \tag{13}$$

an attenuated D'Alembert solution valid for a lossy medium with relatively constant attenuation over the frequency range of the pulse.

We next introduce first-order dispersion terms as a Taylor series approximation over a limited bandwidth, so that $c \equiv c_0 + c_1 \cdot |\omega|$ and $\alpha \equiv \alpha_0 + \alpha_1 \cdot |\omega|$, where $c_0 >> c_1\omega$ and $\alpha_0 >> \alpha_1\omega$. However, for low-pass functions like the Gaussian, the behavior of c and k near zero frequency is particularly important. Under most conventional loss mechanisms (Blackstock 2000), as $\omega \to 0$, $c \to c_0$ and $\alpha \to 0$. Thus, $\alpha_0 = 0$ for low-pass functions in conventional lossy media. By substituting these into eqn (12), again assuming weak attenuation, $\alpha << \omega/c$, and then retaining only the most significant terms, we find

$$\begin{aligned} v_z(x,\omega) &\cong \frac{c_0}{2}\,\mathbf{e}^{-\frac{1}{2}\sigma^2\left(\frac{\omega}{c_0}\right)^2}\mathbf{e}^{-i\left(\frac{\omega}{c_0+c_1|\omega|}\right)x}\mathbf{e}^{-(\alpha_1|\omega|)x} \\ &\cong \frac{c_0}{2}\,\mathbf{e}^{-\frac{1}{2}\sigma^2\left(\frac{\omega}{c_0}\right)^2}\mathbf{e}^{-ix\left[\frac{\omega}{c_0}-\frac{c_1\omega^2\mathrm{sign}[\omega]}{c_0^2}\right]}\mathbf{e}^{-\alpha_1|\omega|x} \end{aligned} \tag{14}$$

where a first-order series expansion $1/(1 + (c_1/c_0)|\omega|) \cong 1 - (c_1/c_0)|\omega|$ is used in the phase term.

Taking the inverse Fourier transform with respect to temporal frequency and rearranging some terms, we obtain

$$v_z(x,t) = \frac{c_0^2}{2\sigma\sqrt{2\pi}}\left[\mathbf{e}^{\frac{-(c_0t-x)^2}{2\sigma^2}}\right] * \left(\frac{1}{\pi}\frac{\alpha_1 x}{t^2+(\alpha_1 x)^2}\right) * \mathrm{Quad}(t) \tag{15}$$

where the asterisks represent convolution, and the term $(1/\pi)(\alpha_1 x/(t^2 + (\alpha_1 x)^2)$ is the inverse Fourier transform (IFT) of $\mathbf{e}^{-\alpha_1|\omega|x}$, essentially a low-pass filter. Quad(t) is the IFT of the quadratic phase term

$$\mathbf{e}^{+ixc_1\frac{\omega^2\mathrm{sign}[\omega]}{c_0^2}}$$

The quadratic phase all-pass filter has significant distortion effects. Its time-domain impulse response, Quad(t), is a type of right-sided chirp. When convolved with a Gaussian, a distortion and warping are produced, with the degree of distortion depending on the magnitude of the quadratic phase term $[x \cdot c_1 \cdot (\omega/c_0)^2]$ over the Gaussian bandwidth σ. Its exact form from Mathematica (Wolfram Research, Champaign, IL, USA) for $x(c_1/c_0^2) = 1$ is

$$\mathrm{Quad}(t) = \frac{1}{2}\left[\cos\left(\frac{t^2}{4}\right)\left(1+2\boldsymbol{C}\left(\frac{t}{\sqrt{2\pi}}\right)\right) + \sin\left(\frac{t^2}{4}\right)\left(1+2\boldsymbol{S}\left(\frac{t}{2\pi}\right)\right)\right] \tag{16}$$

where $\boldsymbol{C}(\cdot)$ and $\boldsymbol{S}(\cdot)$ are the Fresnel cosine and sine integrals, respectively. The result of these convolutions is a waveform that is diminished in amplitude and broadened as it propagates.

Cylindrical coordinate solution: Green's function in an elastic medium

In most cases, the beam in Figure 2 will not be extended in the y-axis, and in the case of an axisymmetric beam, the solution can be found as a function of cylindrical radius, $r = (x^2 + y^2)^{1/2}$. The Laplacian operator in eqn (2) for cylindrical coordinates leads naturally to the Hankel transform (Graff 1975). Unfortunately, the singularity and peculiarities of Bessel functions in Hankel transforms make it very difficult to obtain closed-form solutions involving Gaussian functions. Nonetheless, approximate solutions can be derived and compared with the 1-D solution. The problem begins with a quiescent infinite homogeneous medium and an extended line source of force, along the z-axis at the origin. The resulting solution will have only a non-zero polarized shear wave with displacement and velocity in the z-axis, and non-zero derivatives in the radial dimension.

Applying the Hankel transform $\mathbf{H}$ in space and the Fourier transform in time to eqn (2) in cylindrical coordinates yields

$$\widehat{U}(\varepsilon,\omega) = \frac{\widehat{F}(\varepsilon)}{\varepsilon^2 - \frac{\omega^2}{c^2}} \tag{17}$$

where $\widehat{F}(\varepsilon) = \mathbf{H}[F(r)](\varepsilon)$; ε= spatial frequency; and $\widehat{T}(\omega) = \Im[T(t)] = 1$ assuming an impulse, and

$$\widehat{u}(r,\omega) = \int_0^\infty \frac{\widehat{F}(\varepsilon)}{\varepsilon^2 - \frac{\omega^2}{c^2}} J_0(\varepsilon r)\varepsilon d\varepsilon \tag{18}$$

Now, after application of Baddour's (2011) Theorem 3, the following results hold true:

$$\int_0^\infty \frac{\widehat{F}(\varepsilon)}{\varepsilon^2 - k^2} J_n(\varepsilon r)\varepsilon d\varepsilon = \begin{cases} -\frac{\pi}{2} Y_n(kr)\widehat{F}(k) \\ \pi i \frac{1}{2} H_n^{(1)}(kr)\widehat{F}(k) \\ -\pi i \frac{1}{2} H_n^{(2)}(kr)\widehat{F}(k) \end{cases} \tag{19}$$

Here, $k = \omega/c$ is a real wavenumber, $Y_n(x)$ is a Bessel function of the second kind and $H_n^{(1,2)}(x)$ are Hankel functions of the first and second kind, respectively. In applying this theorem, the Sommerfield radiation condition must be used to select the appropriate solution that yields out-ward propagating waves, the correct application of which depends on the chosen time dependence of the solution, which, in turn, is reflected in the chosen definition of the Fourier transform. In our case, we have stated the chosen definition of the Fourier transform above, and this corresponds to an implied time dependence of $\mathbf{e}^{i\omega t}$, which, in turn, implies that the correct application of the theorem yields

$$\widehat{u}(r,\omega) = \frac{-\pi i}{2} H_0^{(2)}\left(\frac{\omega}{c}\cdot r\right)\widehat{F}\left(\frac{\omega}{c}\right) \tag{20}$$

where

$$u(r,t) = \Im_\omega^{-1}\{\widehat{u}(r,\omega)\} \tag{21}$$

Now, for the specific solutions we first examine the Green's function for a force that is impulsive in space and time. Let $F_z(r)T(t) = A_0\delta(t)\delta(r)/r$, where A_0 is a constant of proportionality; then,

$$\widehat{u}(r,\omega) = A_0\frac{-\pi i}{2} H_0^{(2)}\left(\frac{\omega}{c}\cdot r\right) \tag{22}$$

Note that the general requirement for a causal function $f(t)$ is that $f(t) = 0$ for $t < 0$ (Papoulis 1987), in which case

$$f(t) = \frac{2}{\pi}\int_0^\infty R(\omega)\cos(\omega t)d\omega = -\frac{2}{\pi}\int_0^\infty X(\omega)\sin(\omega t)d\omega \tag{23}$$

where $R(\omega) \equiv$ real part of $\Im\{f(t)\}$, and $X(\omega) \equiv$ imaginary part of $\Im\{f(t)\}$.

Now, for our case,

$$\begin{aligned}\widehat{u}(r,\omega) &= A_0\frac{-\pi}{2}iH_0^{(2)}\left(\frac{\omega}{c}\cdot r\right)\\ &= A_0\frac{-\pi}{2}\left[Y_0\left(\omega\cdot\frac{r}{c}\right)+iJ_0\left(\omega\cdot\frac{r}{c}\right)\right]\end{aligned} \tag{24}$$

So for a causal $u(r, t)$,

$$u(r,t) = A_0\frac{-\pi}{2}\left(\frac{-2}{\pi}\right)\int_0^\infty J_0\left(\omega\bullet\frac{r}{c}\right)\sin(\omega t)d\omega \tag{25}$$

and from Gradshteyn and Ryzhik (1965:73),

$$u(r,t) = A_0\frac{1}{\sqrt{t^2-\left(\frac{r}{c}\right)^2}} \quad \text{for} \quad 0<\frac{r}{c}<t \tag{26}$$

and this agrees with Graff's (1975) solution by Laplace transform.

The corresponding solution for velocity, v, is given by $(d/dt)u(r, t)$:

$$v(r,t) = \frac{A_0\delta\left(t-\frac{r}{c}\right)}{\left(t^2-\frac{r^2}{c^2}\right)^{\frac{1}{2}}}-\frac{A_0 t\cdot H\left(t-\frac{r}{c}\right)}{\left(t^2-\frac{r^2}{c^2}\right)^{\frac{3}{2}}} \tag{27}$$

where $H(\bullet)$ is the Heaviside step function.

Comparing u and v, we see features that were also evident in the 1-D case. The Green's function for u is persistent in time with a $1/t$ decay, which, in experiments, is vulnerable to contamination by ambient vibration and baseline drift and reflections from distant boundaries. The leading edge is a singularity that survives to infinite distances, a result that is experimentally unrealizable. The Green's function for $v(r,t)$ is more promising: it contains a delta function, which will be useful in convolving with and reproducing a beam pattern. Unlike the 1-D case, it has a negative "recoil" term (the second term in eqn [27]), which decays asymptotically as $1/t^2$ and, so, is more localized spatially than u.

We next seek a solution to the Gaussian beam pattern. Let

$$F_z(r)T(t) = \left(\frac{1}{2\sigma^2}\right)\mathbf{e}^{-r^2/4\sigma^2}\delta(t)$$

Then, from eqn (20), and taking the Hankel transform of $F_z(r)$, we have

$$\widehat{u}(r,\omega) = -\pi i\frac{1}{2}H_0^{(2)}\left(\frac{\omega}{c}\cdot r\right)\left[\mathbf{e}^{-\sigma^2\left(\frac{\omega}{c}\right)^2}\right] \tag{28}$$

and the causality constraint, eqn (23), yields

$$u(r,t) = \int_0^\infty J_0\left(\omega\cdot\frac{r}{c}\right)\mathbf{e}^{-\sigma^2\left(\frac{\omega}{c}\right)^2}\sin(\omega t)d\omega \tag{29}$$

or

$$u(r,t) = -\int_0^\infty Y_0\left(\omega\cdot\frac{r}{c}\right)\mathbf{e}^{-\sigma^2\left(\frac{\omega}{c}\right)^2}\cos(\omega t)d\omega \tag{30}$$

or, because $\widehat{v}(r,\omega) = i\omega\widehat{u}(r,\omega)$,

$$v(r,t) = \int_0^\infty \omega\cdot J_0\left(\omega\cdot\frac{r}{c}\right)\mathbf{e}^{-\sigma^2\left(\frac{\omega}{c}\right)^2}\cos(\omega t)d\omega \tag{31}$$

or

$$v(r,t) = \int_0^\infty \omega Y_0\left(\omega\cdot\frac{r}{c}\right)\mathbf{e}^{-\sigma^2\left(\frac{\omega}{c}\right)^2}\sin(\omega t)d\omega \tag{32}$$

No closed-form solutions to these have been found. Alternatively, we could convolve the Green's functions for u or v (eqn [26] and [27]) with a Gaussian in the time domain; however, no closed-form solution has been found for this approach either. We therefore turn to an approximate solution. If as an approximation to the Gaussian we use a similar shape

$$F_z(r)T(t) = \frac{A_0}{(r^2+a^2)^{\frac{1}{2}}}\delta(t) \tag{33}$$

where a is a beamwidth parameter, then

$$\mathbf{H}[F_z(r)] = \frac{A_0\mathbf{e}^{-a\varepsilon}}{\varepsilon} \tag{34}$$

Superficially, this $F_z(r)$ resembles the "bell shape" of the Gaussian beam. An important difference is the relatively slow $1/r$ dropoff, as depicted in Figure 3. This slowly decaying "tail" of the function leads to a singularity in $\mathbf{H}[F_z(r)]$ at zero frequency and to long "tails" in the solutions. Nonetheless, the approximation provides a useful vehicle for examining the effects of dispersion. Substituting eqn (34) into eqn (20) and invoking causality yield

$$u(r,t) = A_0\int_0^\infty J_0\left(\omega\cdot\frac{r}{c}\right)\frac{\mathbf{e}^{-a\left(\frac{\omega}{c}\right)}}{\left(\frac{\omega}{c}\right)}\sin(\omega t)d\omega \tag{35}$$

which can be interpreted as the Fourier sine transform of the function $(c/\omega)\exp(-a(\omega/c))J_0(\omega \cdot r/c)$, which is known as Erdélyi Theorem 17 (Erdélyi and Bateman 1954). Thus,

$$u(r,t) = A_0 c\cdot\sin^{-1}\left(\frac{2t}{r_1+r_2}\right)\text{for} \quad t\geq 0 \quad \text{and} \quad r\geq o \tag{36}$$

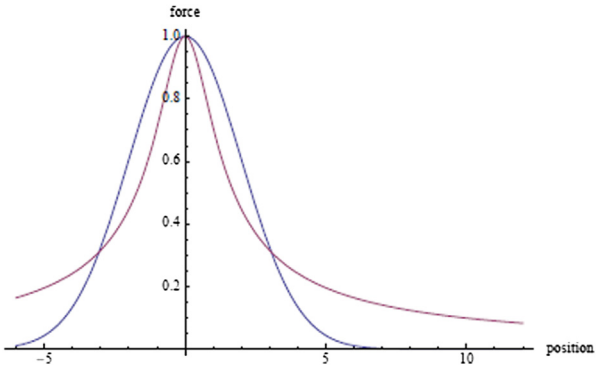

Fig. 3. Comparison of a Gaussian function of $\sigma = 2$ units and a substitute function $1/(r^2 + 1)^{1/2}$, both normalized to unit amplitude at $r = 0$. The substitute function and its Hankel transform lead to an analytical solution that is useful for illustrating the effects of dispersion. However, it has a slow asymptotic decay of $1/r$ and, therefore, much wider "tails" compared with the Gaussian.

where $r_1^2 = (a/c)^2 + (t + r/c)^2$ and $r_2^2 = (a/c)^2 + (t - r/c)^2$, and

$$v_{\text{approx}}(r,t) = \frac{d}{dt}u(r,t) \tag{37}$$

where the subscript designates an approximation, meaning the solution is for a substitute beam pattern, not an exact Gaussian. Because of the long "tails" of the substitute beam pattern and the nature of the cylindrical Green's function, the velocity is extended in time and space.

Cylindrical coordinate solution: Cylindrical coordinates and a dispersive medium

To introduce dispersion, we substitute a complex k and seek a solution. Baddour's Theorem 4 for Bessel functions holds for complex wavenumber (Baddour 2011). This theorem states

$$\int_0^\infty \frac{\widehat{F}(\varepsilon)}{\varepsilon^2 - k^2} J_n(\varepsilon r)\varepsilon d\varepsilon = \begin{cases} \pi i \tfrac{1}{2} H_n^{(1)}(kr)\widehat{F}(k) & \text{Im}(k) > 0 \\ -\pi i \tfrac{1}{2} H_n^{(2)}(kr)\widehat{F}(k) & \text{Im}(k) < 0 \end{cases} \tag{38}$$

Using this theorem along with eqn (34) and complex wavenumber yields

$$u(r,\omega) = -A_0 \frac{\pi i}{2} H_0^{(2)}\left(\frac{\omega}{c} r - i\alpha r\right) \frac{\mathbf{e}^{-a\left(\frac{\omega}{c} - i\alpha\right)}}{\left(\frac{\omega}{c} - i\alpha\right)} \tag{39}$$

The solution should resemble the previous case except for the effects of the imaginary term in the argument. Assuming $\alpha << \omega/c$ and taking only leading terms of $\exp(-a(\omega/c - i\alpha))/(\omega/c - i\alpha)$, leaves us with a real approximation for $\widehat{F}(k) = \exp(-a(\omega/c))/(\omega/c)$, where we also substituted $\text{Re}[\mathbf{e}^{+i\alpha a}] = \cos[a\alpha] \cong 1$ by assuming $a\alpha << 1$. Thus

$$u(r,\omega) = -A_0 \frac{\pi i}{2} H_0^{(2)}\left(\frac{\omega}{c} r - i\alpha r\right) \cdot \frac{\mathbf{e}^{-a\left(\frac{\omega}{c}\right)}}{\left(\frac{\omega}{c}\right)} \tag{40}$$

Now, by adding dispersion to eqn (40), $c = c_0 + c_1|\omega|$, $\alpha = \alpha_1|\omega|$, and by retaining the most significant terms, we have

$$u(r,\omega) = -A_0 \frac{\pi i}{2} \left[H_0^{(2)}\left(\frac{\omega}{c_0} r - \left(\frac{\omega^2 c_1 \text{sign}(\omega)}{c_0^2}\right) r - i(\alpha_1|\omega|)r\right)\right] \frac{\mathbf{e}^{-a\left(\frac{\omega}{c_0}\right)}}{\left(\frac{\omega}{c_0}\right)} \tag{41}$$

Consider the asymptotic form for $H_0^{(2)}$ (Abramowitz and Stegun 1964) for complex z:

$$H_0^{(2)}(z) \cong \sqrt{\frac{2}{\pi z}} \mathbf{e}^{-i\left(z - \frac{\pi}{4}\right)} \tag{42}$$

Now if $z = a - ib$ and $0 < b << a$, then eqn (42) suggests a useful approximation, $H_0^{(2)}(a - ib) \cong \mathbf{e}^{-b} H_0^{(2)}(a)$, and it can be verified that this approximation works well over all real, positive a, as long as $b << a$. Substituting this into eqn (41) yields

$$u(r,\omega) \cong -A_0 \frac{\pi i}{2} \mathbf{e}^{-(\alpha_1|\omega|)r} \cdot H_0^{(2)}\left(\left[\frac{\omega}{c_0} - \left(\frac{\omega}{c_0}\right)^2 c_1 \text{sign}(\omega)\right] r\right) \cdot \frac{\mathbf{e}^{-a\left(\frac{\omega}{c_0}\right)}}{\left(\frac{\omega}{c_0}\right)} \tag{43}$$

Similarly, by substituting $z = (ax - bx^2)$ into eqn (42), we have found that $H_0^{(2)}(ax - bx^2)$ is well approximated by a chirp of the form

$$H_0^{(2)}\left(ax - bx^2\right) \cong H_0^{(2)}(ax) \left[\frac{1}{1 - \frac{bx}{a}}\right]^{\frac{1}{2}} \mathbf{e}^{+ibx^2} \quad \text{for} \quad x > 0 \quad \text{and} \quad a > b > 0 \tag{44}$$

Thus,

$$u(r,\omega) \cong -A_0 \frac{\pi i}{2}\, \mathbf{e}^{-\alpha_1|\omega|r} \cdot H_0^{(2)}\left(\frac{\omega}{c_0} r\right) \cdot \left[\frac{c_0}{c_0 - c_1|\omega|}\right]^{\frac{1}{2}} \cdot \mathbf{e}^{+i\left(\frac{\omega}{c_0}\right)^2 \mathrm{sign}(\omega) c_1 r} \cdot \frac{\mathbf{e}^{-a\left(\frac{\omega}{c_0}\right)}}{\left(\frac{\omega}{c_0}\right)} \quad \text{for} \quad r>0 \tag{45}$$

Note that the kernel of this expression

$$H_0^{(2)}\left(\frac{\omega}{c} r\right) \cdot \frac{\mathbf{e}^{-a\left(\frac{\omega}{c_0}\right)}}{\left(\frac{\omega}{c_0}\right)}$$

is that which was obtained for the lossless, elastic case (eqns [20] and [34]). The other terms resemble those observed in the 1-D case (eqn [14]), an exponential decay with frequency and a quadratic phase distortion. There is an additional amplitude term associated with cylindrical dispersive spreading proportional to $[c_0/(c_0 - c_1|\omega|)]^{1/2}$; however, assuming $\omega c_1 << c_0$, , this term is $\cong 1$ over the bandwidth of the pulse. Thus, in the time domain we conclude that

$$v(r,t) \cong \left[v_{\text{approx}}(r,t)\right] * \frac{1}{\pi} \frac{\alpha_1 r}{\left(t^2 + (\alpha_1 r)^2\right)} * \text{Quad}(t) \tag{46}$$

for a dispersive medium where $v_{\text{approx}}(r,t)$ is defined by eqns (36) and (37). Note that eqn (46) has the same structure as eqn (15) for the 1-D case, suggesting the possibility of a common convolution term for modeling dispersion.

RESULTS

The solutions are evaluated with parameters that approximate soft biomaterials (Zhang et al. 2007). For the lossless cases, $c_0 = 2$ m/s and a 1-mm beamwidth Gaussian parameter is used. For lossy and dispersive media, we additionally include $c_1 = 0.1$ mm/s/Hz (in other words, the speed rises linearly from 2.00 m/s at low frequencies to 2.01 m/s at 100 Hz), and $\alpha_1 = 1 \times 10^{-4}$ Np/mm/Hz (in other words the attenuation coefficient is 0.1 Np/cm at 100 Hz). These values are somewhat less dispersive than those found in liver tissue (Barry et al. 2012; Hah et al. 2012; Zhang et al. 2007); however, these values of dispersion are sufficient to show marked changes in the propagating waveforms, compared with the lossless reference cases. Figure 4a provides the time history of velocity at regularly spaced observation points out to 8 mm, for the 1-D solution of the right-traveling shear wave. Because this is essentially D'Alembert's solution, there is no change in the characteristics as the shear wave propagates. Peak tracking would provide an accurate estimation of shear velocity in this case. In Figure 4b is the solution in the dispersive medium, at the same observation points, derived from numerical integration of the inverse Fourier transform of eqn (14). The loss of amplitude and spreading of the shear wave are evident, and this is progressive as the dispersive effects accumulate. The effects of attenuation, which acts as a low-pass filter, are pronounced. For the 8-mm observation point (the rightmost curve) the peak has shifted from 4 ms in the lossless case to approximately 3.7 ms, a drop of 10% caused by relatively modest loss parameters. Figure 5 provides the results for a cylindrically symmetric beam. The time history is shown at observation points identical to those in Figure 4, at regular spacings

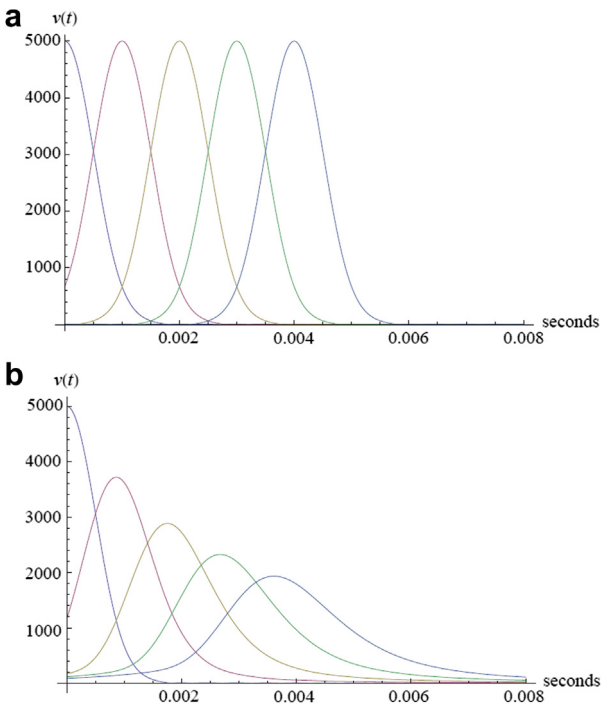

Fig. 4. Theoretical values of velocity (arbitrary units)-versus-time (s) profiles for the right-traveling shear wave of the 1-D case, at observation points 0, 2, 4, 6 and 8 mm from the center of the Gaussian beam. (a) Simple case of the lossless medium, reducing to D'Alembert's solution. (b) Same initial beam and observation points, but with modest loss and dispersion characteristic of some soft tissues.

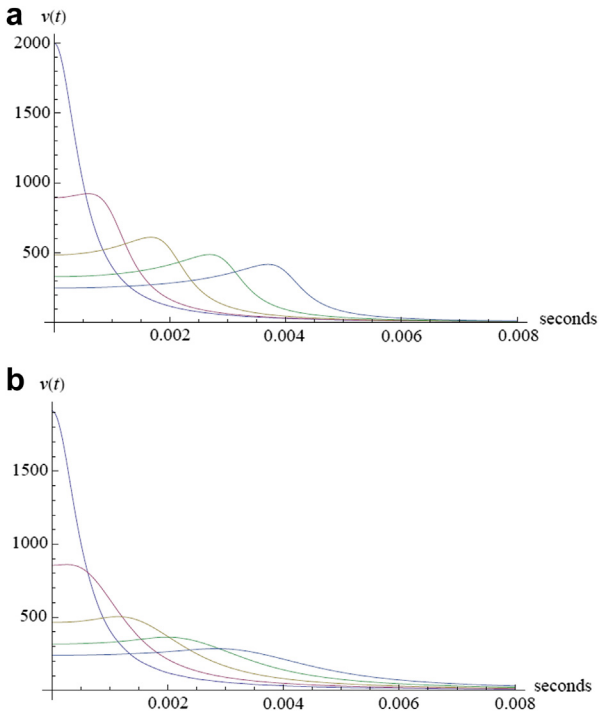

Fig. 5. Theoretical values of velocity (arbitrary units)-versus-time (s) profiles for the shear wave of the cylindrical case, at observation points 0, 2, 4, 6 and 8 mm radially from the center of an approximately Gaussian beam. (a) Rapid initial loss of amplitude followed by cylindrical spreading is seen even in the lossless case. (b) With dispersion, the smoothing of the waveforms and amplitude losses are pronounced.

out to 8 mm. Solutions are obtained by numerical integration of the inverse Fourier transform of eqn (45). In the lossless case (Fig. 5a), the rapid decrease in amplitude followed by the asymptotic approach to $1/\sqrt{r}$ cylindrical spreading is demonstrated. With dispersion (Fig. 5b), the low-pass smoothing of the velocity waveforms is evident. These waveforms are more extended than in the 1-D case because of the cylindrical Green's function and because the approximation to a Gaussian function, with slower convergence, was used in the closed-form analytic solution to eqns (28)–(36). In this example, the 8-mm observation point (rightmost curve) has a peak near 3.8 ms in the lossless case, dropping to 3.1 ms in the lossy case (Fig. 5b). Neither case has the simple value of 4 ms expected from consideration of a plane wave in a lossless medium. The combined effects of dispersion and cylindrical spreading in eqn (46) are complicated; for example, higher-temporal-frequency components are traveling faster, but are also more highly attenuated. It should also be noted that the experimental task of finding a "peak" becomes quite difficult for dispersive examples like that in Figure 5b, even more so in the presence of noise.

DISCUSSION AND CONCLUSIONS

Closed-form analytical expressions have been derived for the case of a Gaussian shear wave in a lossy, dispersive medium. The framework for solving inverse transforms employs the recent theorems published by Baddour (2011). In all cases, a general first-order approximation to dispersion is employed, so the results are not tied to any particular model of tissue loss. In the resulting solutions, one key term that drives the distortion and diminution of the wave is a low-pass filter term resulting from the progressively higher attenuation of higher frequencies as a result of dispersion. Another key term is the quadratic phase term resulting from the progressively higher wave speed as a result of dispersion. Some specific results of interest emerge from the analysis:

- By extending the beam in the out-of-plane dimension, an approximate 1-D configuration is generated. This leads to the simplest solution, D'Alembert's solution, where the shape of the beam pattern is carried by the velocity wave, not the displacement wave.
- The displacement wave has a long "tail" that is not well confined in space and time, and is dependent on low-frequency terms that are difficult to know *a priori*; thus, the velocity wave is better suited for tracking.
- In cylindrical coordinates, a dramatic initial drop in the velocity wave is followed by the $1/\sqrt{r}$ cylindrical decay, plus additional terms caused by dispersion.
- The cylindrical Green's function contains a negative "recoil" term (eqn [27]); however, after convolution with a beam pattern term, the solution may or may not contain a negative velocity region. This depends on the particular shape of the beam pattern and its compactness.
- In all cases, the unwanted quadratic phase term can be eliminated from consideration by taking the power spectrum of the velocity pulse
- Some approximations for Hankel functions of complex arguments and quadratic arguments are proposed and used within solutions.

These factors help to characterize the rapid diminution and distortion of shear wave pulses in lossy tissue, and suggest approaches to more robust tracking.

Some key limitations of this study should be highlighted for further research. First, dispersion relations assume only a first-order approximation. Next, the approximate solution to the Gaussian shear wave in cylindrical coordinates, eqn (37), is from a "similar" beam pattern. It is useful in demonstrating the extra terms that must be included in a dispersive medium, as opposed to a simple elastic medium. The dispersive terms can be generalized to apply to other beam patterns. However, finding an exact closed-form analytical solution to

eqn (29), (30), (31) or (32) with exact Gaussians is still desirable. Another important limitation of this study is the assumed uniformity of the beam and radiation force in (y, z) or (z) axes for the 1-D and cylindrical cases, respectively. In reality, the beam will have finite extent in the y-direction and a diffraction pattern in the z-axis with progressive attenuation loss. These spatial factors will add additional decay terms to the solutions, further diminishing the propagating shear wave as time increases.

Acknowledgments—We are deeply indebted to Al Clark, David Blackstock and Paul Barbone for their expertise and kind forbearance throughout many interruptions and questions. The expertise of Dr. Zaegyoo (Jay) Hah in generating the data for Figure 1 is gratefully acknowledged. This work was supported in part by National Institutes of Health Grant 5 R01 AG02980-04, by the University of Rochester Department of Electrical and Computer Engineering and by the National Science and Engineering Research Council of Canada.

REFERENCES

Abramowitz M, Stegun IA. Handbook of mathematical functions with formulas, graphs, and mathematical tables. Washington, DC: U.S. Government Printing Office; 1964.

Baddour N. Multidimensional wave field signal theory: Mathematical foundations. AIP Advances 2011;1:022120.

Barry CT, Mills B, Hah Z, Mooney RA, Ryan CK, Rubens DJ, Parker KJ. Shear wave dispersion measures liver steatosis. Ultrasound Med Biol 2012;38:175–182.

Bercoff J, Tanter M, Fink M. Supersonic shear imaging: A new technique for soft tissue elasticity mapping. IEEE Trans Ultrason Ferroelectr Freq Control 2004a;51:396–409.

Bercoff J, Tanter M, Muller M, Fink M. The role of viscosity in the impulse diffraction field of elastic waves induced by the acoustic radiation force. IEEE Trans Ultrason Ferroelectr Freq Control 2004b;51:1523–1536.

Blackstock DT. Fundamentals of physical acoustics. New York: Wiley; 2000. ch 9.

Chen S, Fatemi M, Greenleaf JF. Quantifying elasticity and viscosity from measurement of shear wave speed dispersion. J Acoust Soc Am 2004;115:2781–2785.

Chen W, Holm S. Modified Szabo's wave equation models for lossy media obeying frequency power law. J Acoust Soc Am 2003;114:2570–2574.

Chen W, Holm S. Fractional Laplacian time-space models for linear and nonlinear lossy media exhibiting arbitrary frequency power-law dependency. J Acoust Soc Am 2004;115:1424–1430.

Doyley MM. Model-based elastography: A survey of approaches to the inverse elasticity problem. Phys Med Biol 2012;57:R35–R73.

Erdélyi A, Bateman H. Tables of integral transforms. Vol. 1. New York: McGraw-Hill; 1954. p. 101.

Fahey BJ, Nightingale KR, McAleavey SA, Palmeri ML, Wolf PD, Trahey GE. Acoustic radiation force impulse imaging of myocardial radiofrequency ablation: Initial in vivo results. IEEE Trans Ultrason Ferroelectr Freq Control 2005;52:631–641.

Fatemi M, Greenleaf JF. Ultrasound-stimulated vibro-acoustic spectrography. Science 1998;280:82–85.

Giannoula A, Cobbold RSC. Narrowband shear wave generation by a finite-amplitude radiation force: The fundamental component. IEEE Trans Ultrason Ferroelectr Freq Control 2008;55:343–358.

Giannoula A, Cobbold RSC. Propagation of shear waves generated by a modulated finite amplitude radiation force in a viscoelastic medium. IEEE Trans Ultrason Ferroelectr Freq Control 2009;56:575–588.

Gradshteyn IS, Ryzhik IM. Tables of integrals series, and products. San Diego: Academic Press; 1965.

Graff KF. Wave motion in elastic solids. Oxford: Clarendon Press; 1975. p. 283–288.

Hah Z, Hazard C, Mills B, Barry C, Rubens D, Parker K. Integration of crawling waves in an ultrasound imaging system: Part 2. Signal processing and applications. Ultrasound Med Biol 2012;38:312–323.

Hazard C, Hah Z, Rubens D, Parker K. Integration of crawling waves in an ultrasound imaging system: Part 1. System and design considerations. Ultrasound Med Biol 2012;38:296–311.

Konofagou EE, Hynynen K. Localized harmonic motion imaging: Theory, simulations and experiments. Ultrasound Med Biol 2003;29:1405–1413.

McAleavey S, Menon M. 7B-3 Direct estimation of shear modulus using spatially modulated acoustic radiation force impulses. In: Proceedings, 2007 IEEE International Ultrasonics Symposium, New York, 28–31 October. New York: IEEE, 2007:558–561.

Nachman AI, Smith JF, Waag RC. An equation for acoustic propagation in inhomogeneous-media with relaxation losses. J Acoust Soc Am 1990;88:1584–1595.

Nightingale K, Nightingale R, Palmeri M, Trahey G. Finite element analysis of radiation force induced tissue motion with experimental validation. In: Proceedings, IEEE International Ultrasonics Symposium, Caesar's Tahoe, Nevada, 17–20 October. Vol. 2. New York: IEEE, 1999:1319–1223 vol. 2.

Nightingale KR, Palmeri ML, Nightingale RW, Trahey GE. On the feasibility of remote palpation using acoustic radiation force. J Acoust Soc Am 2001;110:625–634.

Papoulis A. The Fourier integral and its applications. New York: McGraw-Hill; 1987. p. 11.

Parker KJ, Doyley MM, Rubens DJ. Imaging the elastic properties of tissue: The 20 year perspective. Phys Med Biol 2011;56:R1–R29.

Sarvazyan AP, Rudenko OV, Swanson SD, Fowlkes JB, Emelianov SY. Shear wave elasticity imaging: A new ultrasonic technology of medical diagnostics. Ultrasound Med Biol 1998;24:1419–1435.

Szabo TL. Time-domain wave-equations for lossy media obeying a frequency power-law. J Acoust Soc Am 1994;96:491–500.

Urban MW, Chen SG, Greenleaf JF. Error in estimates of tissue material properties from shear wave dispersion ultrasound vibrometry. IEEE Trans Ultrason Ferroelectr Freq Control 2009;56:748–758.

Zhang M, Castaneda B, Wu Z, Nigwekar P, Joseph JV, Rubens DJ, Parker KJ. Congruence of imaging estimators and mechanical measurements of viscoelastic properties of soft tissues. Ultrasound Med Biol 2007;33:1617–1631.